

A small dispersion limit to the Camassa–Holm equation: A numerical study

Jennifer Gorsky^{a,*}, David P. Nicholls^b

^a Department of Mathematics and Computer Science, University of San Diego, 5998 Alcalá Park, San Diego, CA 92110, United States

^b Department of Mathematics, Statistics, and Computer Science, University of Illinois at Chicago, Chicago, IL 60607, United States

Available online 18 June 2009

Abstract

In this paper we take up the question of a small dispersion limit for the Camassa–Holm equation. The particular limit we study involves a modification of the Camassa–Holm equation, seen in the recent theoretical developments by Himonas and Misiólek, as well as the first author, where well-posedness is proved in weak Sobolev spaces. This work led naturally to the question of how solutions actually behave in these modified equations as time evolves. While the dispersive limit studied here is inspired by the work of Lax and Levermore on the zero dispersion limit of the Korteweg–de Vries equation to the inviscid Burgers’ equation, here there is no known Inverse Scattering theory. Consequently, we resort to a sophisticated numerical simulation to study two representative (one smooth and one peakon), but by no means exhaustive, initial conditions in the modified Camassa–Holm equation. In both cases there appears to be a strong limit of the modified Camassa–Holm equation to the Camassa–Holm equation as the dispersive parameter tends to zero, provided that solutions have not evolved for too long (time sufficiently small). For the smooth initial condition considered, this time must be chosen before the solution approaches steepening; beyond this time the computed solution becomes increasingly complicated as the dispersive term tends towards zero, and there does not appear to be a limit. By contrast, for the peakon initial condition this limit does appear to exist for all times considered. While in many cases the computations required few discretization points, there were some very challenging cases (particularly for the small dispersion computations) where an enormous number of unknowns were required to properly resolve the solution.

© 2009 IMACS. Published by Elsevier B.V. All rights reserved.

Keywords: Camassa–Holm equation; Nonlinear dispersive wave equations; Spectral methods; Small-dispersion limits

1. Introduction

In [6] Camassa and Holm found a nonlinear dispersive wave equation which possesses the remarkable property of being completely integrable with soliton solutions that have “peaked” features. This wave equation,

$$\partial_t v + v \partial_x v + (1 - \partial_x^2)^{-1} \partial_x \left[v^2 + \frac{1}{2} (\partial_x v)^2 \right] = 0, \quad (1.1)$$

meant to simulate water waves in the limit of disappearing depth (please see Johnson [19] for a clarification of this statement), was first derived by Fuchssteiner and Fokas [12] but is generally referred to as the Camassa–Holm (CH) equation, while the peaked solitons are called “peakons.” These peakons are noteworthy because they do not have the smoothness properties of, e.g., the solitons for the Korteweg–de Vries (KdV) or the Nonlinear Schrödinger (NLS)

* Corresponding author. Tel.: +619 260 7986; fax: +1 619 260 4293.

E-mail address: jgorsky@sandiego.edu (J. Gorsky).

equations, but rather are quite singular being C^0 but not C^1 . Despite their interesting features, one can easily imagine that the weak smoothness properties of these solutions can pose severe difficulties for both rigorous analysis and numerical simulation of the CH equation. For this reason it is natural to consider a “smoothing” of the CH equation which might mollify these effects.

Inspired by the work of Lax and Levermore [21–24] who studied the inviscid Burgers’ equation,

$$\partial_t v + v \partial_x v = 0, \tag{1.2}$$

and its dispersive regularization,

$$\partial_t v + v \partial_x v + \varepsilon \partial_x^3 v = 0, \tag{1.3}$$

the “weakly dispersive” KdV equation, we investigate in this paper a dispersive regularization of the CH equation, the “modified Camassa–Holm” (mCH) equation,

$$\partial_t v + \varepsilon \partial_x^3 v + v \partial_x v + (1 - \partial_x^2)^{-1} \partial_x \left[v^2 + \frac{1}{2} (\partial_x v)^2 \right] = 0. \tag{1.4}$$

Of course, this is not the only dispersive regularization that one can consider. In fact, the work of Abenda and Grava [2] and Abenda, Grava, and Klein [1] presents the derivation and analysis of the Whitham modulation equations for the CH equation. Our particular regularization is chosen as it enables one to study the well-posedness of the mCH equation in weak Sobolev spaces (see Section 2). Our study is in response to the very natural question: How *do* solutions evolve in this new, modified CH equation? More specifically, do solutions of (1.4) converge to solutions of (1.1) as $\varepsilon \rightarrow 0$, and, if so, on what time interval?

The same question was asked, and answered, by Lax and Levermore [22] in their study of the limit of the weakly dispersive KdV equation (1.3) to the inviscid Burgers’ equation (1.2). However, they were able to appeal to the deep and powerful technique of Inverse Scattering [3] and use it in a fundamental way to produce their analysis of the nature of the convergence of solutions of (1.3) to (1.2). By contrast, this theory appears absent for the mCH equation, and thus it seems one must resort to sophisticated numerical simulations to learn something about this limit. Additionally, the question we have set for ourselves is far too broad and therefore we consider the more manageable task of studying two (but by no means exhaustive) initial profiles in the limit as the dispersive parameter $\varepsilon \rightarrow 0$. The profiles are a cosine and a peakon, and the values of $\varepsilon = 10^{-1}, 10^{-3}, 10^{-5}, 0$ are selected to investigate the small dispersion limit.

In both cases there appears to be an L^∞ (at least) limit of the mCH equation to the CH equation as ε approaches zero, provided that t is sufficiently small. For the smooth profile this t must be chosen *before* the solution approaches steepening. Beyond this time the computed solution becomes increasingly complicated as ε approaches zero and there does not appear to be a limit. By contrast, for the peakon profile this limit *does* appear to exist for all times considered despite its severe lack of smoothness. While in many cases the computations required few discretization points, there were some very challenging cases (particularly for $\varepsilon = 10^{-5}, 0$) where an *enormous* number of unknowns were required to properly resolve the solution.

The organization of the paper is as follows: in Section 2 we discuss theoretical results regarding solutions of both the CH and mCH equations including the well-posedness theory and the peakon solutions. In Section 3 numerical results are presented, including a discussion of the numerical method (Section 3.1), a convergence study (Section 3.2), and a study of the evolution of two initial conditions (Sections 3.3 and 3.4) for mCH as ε approaches zero. Concluding remarks are given in Section 4.

2. Theory

Before beginning the numerical investigation we recall some known theoretical results for the CH and mCH equations. In particular, we review the well-posedness theory of the periodic problem in weak Sobolev spaces which inspired the particular modification found in (1.4) as the dispersive correction to the CH equation. A good starting point is the survey article by Molinet [26] on well-posedness results for CH on the line. For the specific case of CH satisfying periodic boundary conditions the recent paper of Himonas and Misiołek [18] provides an excellent summary of known results. In particular (see Theorem 1.1 of [18]), if the initial data $v(x,0)$ is 2π -periodic and lies in the Sobolev class $H^s([0,2\pi])$, then, if $s > 3/2$, (1.1) is locally well-posed in $H^s([0,2\pi])$ with solutions depending continuously on

the initial data [11,17,25]. Furthermore, as the H^1 norm of solutions to CH is conserved, these solutions exist globally in time (see [16]).

Regarding the mCH equation far less is known. However, using the techniques of Bourgain [4,5], Himonas and Misiolek showed that the mCH equation ($\varepsilon = 1$) is locally well-posed in $H^s([0,2\pi])$ for $s > 1/2$ [16]. Using the techniques of Kenig, Ponce, and Vega [20], one of the authors has extended this result to $s = 1/2$ for small initial data [13,14]. Again, the H^1 norm of solutions of the mCH equation is conserved [16].

In addition to the results given above, the CH equation admits a family of continuous, but not everywhere differentiable, traveling solutions, the peakons. For any $c > 0$, given the initial data

$$\varphi_c(x) = c \sum_{n=-\infty}^{\infty} e^{-|x+2\pi n|} = c \frac{\cosh(\pi - x)}{\sinh(\pi)}, \tag{2.1}$$

on the interval $[0,2\pi]$, (1.1) has the solution

$$v_c(x, t) = c \sum_{n=-\infty}^{\infty} e^{-|x+2\pi n-ct|}, \tag{2.2}$$

see [6,8,9,27,17]. These peakons have all the properties of a soliton, including elasticity of collision between two peakons of different velocities.

3. Numerics

In this section we briefly outline our numerical scheme, a fourth order Integrating-Factor Runge-Kutta technique (see, e.g., [10]) coupled to a Fourier collocation spectral method [7]. Using this algorithm two initial conditions (cosine and peakon) are evolved in the modified Camassa–Holm equation, (1.4), as $\varepsilon \rightarrow 0$. Evidence is presented to substantiate our claim that this algorithm produces reliable results, and then plots of the solution are displayed to indicate the behavior of solutions as time evolves.

3.1. The scheme

Simply put, the numerical scheme is a Fourier spectral collocation of the spatial variable coupled to a fourth order Integrating-Factor Runge-Kutta method for the time discretization [15,7,10]. In more detail, a grid of N_x evenly spaced collocation points, x_j , is specified on the interval $[0,L]$ ($L = 2\pi$ for the remainder of the paper) and the mCH equation, (1.4), is enforced at each of these x_j . In “wavenumber space,” derivatives and non-local operators such as $(1 - \partial_x^2)^{-1}$ can be applied trivially (the latter with a division by $(1 + k^2)$ at each wavenumber).

Working in wavenumber space also has the effect of transforming the linear operator $(-\varepsilon \partial_x^3)$ to scalar multiplication by $-\varepsilon(ik)^3$ so that the exact solution $\hat{u}_k(t)$ of the Fourier transformed *linear* mCH equation,

$$\partial_t \hat{u}_k = -\varepsilon(ik)^3 \hat{u}_k,$$

can be written as

$$\hat{u}_k(t) = \Phi_k(t) \hat{u}_k(0), \quad \Phi_k(t) := e^{-\varepsilon(ik)^3 t}.$$

The Integrating-Factor method amounts to writing each unknown Fourier coefficient of the *full* mCH equation, (1.4), as $\hat{v}_k(t) = \Phi_k(t) w_k(t)$, and noting that the $w_k(t)$ satisfy

$$\partial_t w_k(t) = -\Phi_k(-t) \hat{F}_k(\Phi_k(t) w_k(t)), \tag{3.1}$$

where, from (1.4), \hat{F}_k is the Fourier transform of

$$F(v; t) = v \partial_x v + (1 - \partial_x^2)^{-1} \partial_x \left[v^2 + \frac{1}{2} (\partial_x v)^2 \right].$$

This system of ODEs, (3.1), which features no high-order derivatives (and thus no substantial stiffness), is now integrated with a standard fourth order Runge-Kutta method from $t = 0$ to $t = T$ in N_t time-steps of length $dt = T/N_t$.

Table 1

Cauchy convergence results (fixed $N_x = 512$ and varying N_t) for solution of mCH equation with cosine initial data, dispersion parameter $\varepsilon = 10^{-1}$, and final time $T = 0.5$.

N_x	N_t	L^∞ error
512	188	3.89501×10^{-10}
512	250	3.61471×10^{-11}
512	375	1.36232×10^{-11}
512	500	2.30127×10^{-12}
512	750	8.55982×10^{-13}
512	1000	1.45439×10^{-13}

The final specification is how the products in \hat{F}_k are computed. These are accomplished quickly on the “physical side” with the Fast Fourier Transform (FFT) algorithm [15,7]. In order to stabilize the computations, dealiased products are computed by using zero-padded arrays of length $2N_x$.

3.2. Numerical simulations: convergence

Before proceeding with the numerical simulations we present some evidence that our algorithm is working correctly. Tables 1 and 2 list, for the current ($N^{(j)}$ discretization points) and previous ($N^{(j-1)}$ discretization points) refinement levels, the “ L^∞ error”

$$E_{N^{(j)}} := |v_{N^{(j)}} - v_{N^{(j-1)}}|_{L^\infty}, \quad N^{(j)} = N_t^{(j)}, N_x^{(j)}. \tag{3.2}$$

In Table 1 we have refined N_t with an N_x chosen so large that the spatial error is negligible, and vice versa for Table 2. While measuring Cauchy convergence rather than convergence directly, for a convergent scheme, $E_{N^{(j)}}$ must tend to zero as $N^{(j)} = N_x^{(j)}$ and $N^{(j)} = N_t^{(j)}$ go to infinity. Furthermore, the numerical analysis of partial differential equations [7] indicates that this rate should be

$$E_{N_t^{(j)}} = \mathcal{O}((N_t^{(j)})^{-4}), \quad E_{N_x^{(j)}} = \mathcal{O}(e^{-\alpha N_x^{(j)}}), \quad \alpha > 0, \tag{3.3}$$

for smooth solutions.

Tables 1 and 2 come from the simulation of the mCH equation with $\varepsilon = 0.1$, final time $T = 0.5$ (which is well before any steepening of the solution, see Section 3.3), and initial condition $v(x,0) = \cos(x)$. A careful inspection of Table 1 using a linear least-squares fit to the logarithm of N_t versus the logarithm of the L^∞ error reveals a slope of -4.636 which is in good agreement with (3.3). Regarding the spatial convergence, from Table 2 we see that if N_x is plotted versus the logarithm of the L^∞ error, the resulting graph displays linear behavior. In fact, a linear least-squares fit of N_x to the logarithm of the L^∞ error reveals a slope of -0.5191 . These observations agree well with the prediction, (3.3), of a spectral rate of convergence.

Table 2

Cauchy convergence results (fixed $N_t = 1000$ and varying N_x) for solution of mCH equation with cosine initial data, dispersion parameter $\varepsilon = 10^{-1}$, and final time $T = 0.5$.

N_x	N_t	L^∞ error
12	1000	0.0457843
16	1000	0.00427541
24	1000	0.000255558
32	1000	9.90561×10^{-7}
48	1000	2.67796×10^{-9}
64	1000	3.63043×10^{-14}

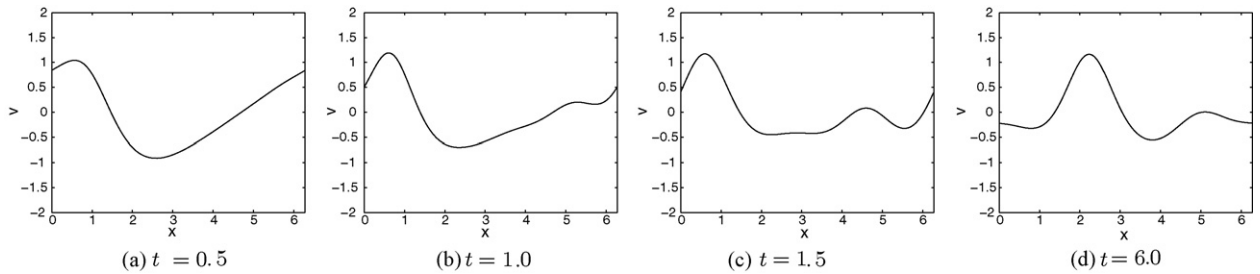


Fig. 1. Evolution of cosine initial data for mCH with $\varepsilon = 10^{-1}$ and 2π -periodic boundary conditions. Numerical parameters are $N_x = 512$ and $dt = 5 \times 10^{-4}$.

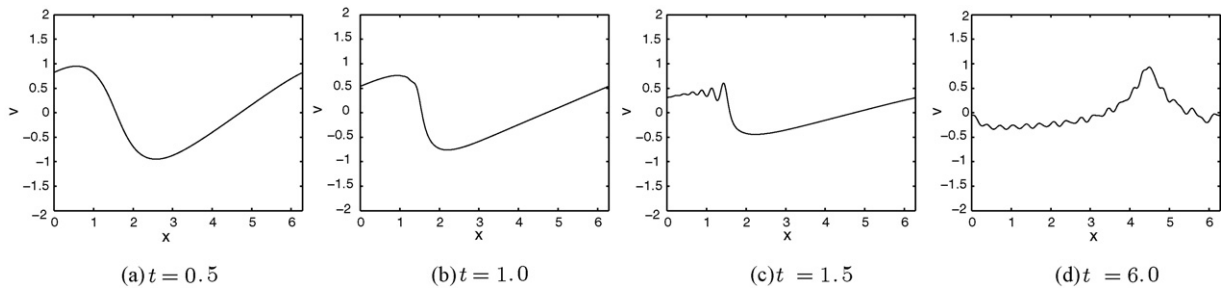


Fig. 2. Evolution of cosine initial data for mCH with $\varepsilon = 10^{-3}$ and 2π -periodic boundary conditions. Numerical parameters are $N_x = 512$ and $dt = 5 \times 10^{-4}$.

3.3. Numerical simulations: cosine profile

To begin the numerical investigations, consider an initial profile shaped as a cosine. In an attempt to standardize and nondimensionalize the results we will take, as we mentioned before, $L = 2\pi$, while also choosing unit amplitude of the initial data, thus $v(x,0) = \cos(x)$. The cosine is a convenient starting point due to its smoothness and the fact that its representation in Fourier space is concentrated entirely at wavenumbers $k = \pm 1$.

Beginning with a (relatively) large value of the dispersion parameter $\varepsilon = 10^{-1}$, by choosing $N_x = 512$ and $N_t = 12,000$ one can realize an error, c.f. (3.2), of 7.98606×10^{-12} at the final time $T = 6.0$. Fig. 1 displays plots of the solution of mCH with $\varepsilon = 10^{-1}$ and cosine initial data at times $t = 0.5, 1.0, 1.5,$ and 6.0 . The computation could have been continued for much longer, however, the simulation was ended here as it displays all of the essential features of this evolution while giving a final time comparable to the length of the period interval. In all future runs we have endeavored to reach this same final time for consistency, and only mention the final time if it differs from $T = 6.0$. Note that all subsequent errors will be computed at the final time. In this simulation the profile steepens initially but this is then mollified by the introduction of a rather large-scale oscillation. Here the features of the solution are smooth and easily resolved using far fewer than the $N_x = 512$ points we have chosen.

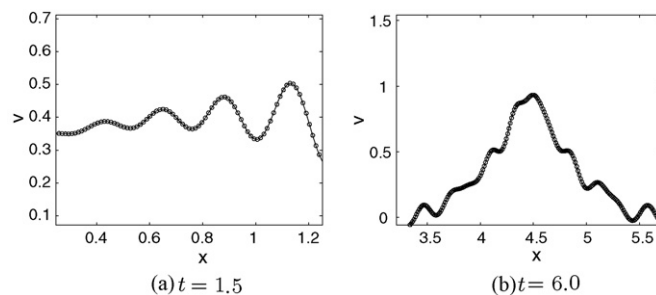


Fig. 3. Magnification of Fig. 2(c) and (d) (mCH with $\varepsilon = 10^{-3}$, 2π -periodic boundary conditions, $N_x = 512$, and $dt = 5 \times 10^{-4}$).

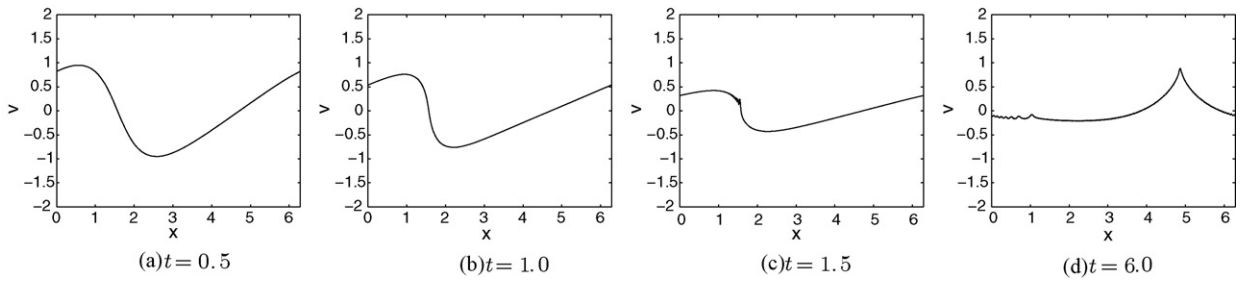


Fig. 4. Evolution of cosine initial data for mCH with $\varepsilon = 10^{-5}$ and 2π -periodic boundary conditions. Numerical parameters are $N_x = 4096$ and $dt = 5 \times 10^{-4}$.

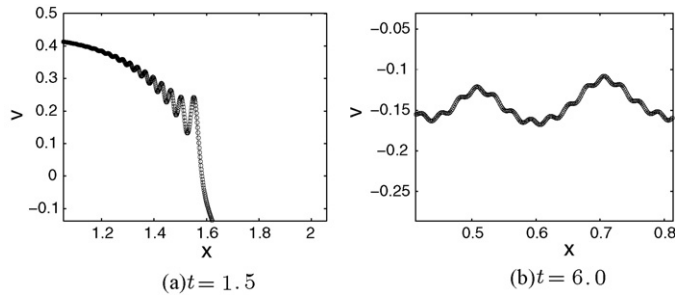


Fig. 5. Magnification of Fig. 4(c) and (d) (mCH with $\varepsilon = 10^{-5}$, 2π -periodic boundary conditions, $N_x = 4096$, and $dt = 5 \times 10^{-4}$).

Next, the calculations above were reconsidered in the case $\varepsilon = 10^{-3}$. Here one can achieve an error of 9.01067×10^{-9} with $N_x = 512$ and $N_t = 12,000$. Fig. 2 displays the solution of mCH with $\varepsilon = 10^{-3}$ and cosine initial data at times $t = 0.5, 1.0, 1.5,$ and 6.0 . We note the markedly different behavior from the solution in the case $\varepsilon = 10^{-1}$. Again, the solution begins by steepening and appears to be smoothed when the slope becomes too steep. However, this oscillation is of significantly higher frequency and eventually leads to a solution with quite a complicated structure. One could wonder if these solutions are well-converged, but for this we appeal to the magnifications of the solutions at $t = 1.5$ and 6.0 displayed in Fig. 3. Here one sees that the high frequency content is genuine and not a numerical artifact.

Moving to mCH with $\varepsilon = 10^{-5}$ and the cosine profile, an accuracy of 0.000359156 can be found with $N_x = 4096$ and $N_t = 12,000$. While this error is somewhat larger than that presented above, it is still quite acceptable at 10^{-4} . Fig. 4 exhibits the drastically different behavior for $\varepsilon = 10^{-5}$. Once again we see the initial steepening followed by a rapid dispersion of the sharp gradient. Again, the magnified pictures, Fig. 5, give evidence of the convergence of the solutions. However, rather than progressing to a smooth profile as in the case $\varepsilon = 10^{-1}$, the solution moves towards a peaked profile. This appears to progress stably though it is clearly rather difficult to resolve.

Finally, we consider the evolution of the cosine profile in the CH equation (mCH with $\varepsilon = 0$). This was an extremely challenging simulation which required $N_x = 16,384$ and $N_t = 24,000$ to achieve accuracy 0.00847588 . Here the evolution is remarkably different from the cases with $\varepsilon > 0$, see Fig. 6. Once again there is an initial steepening which is resolved

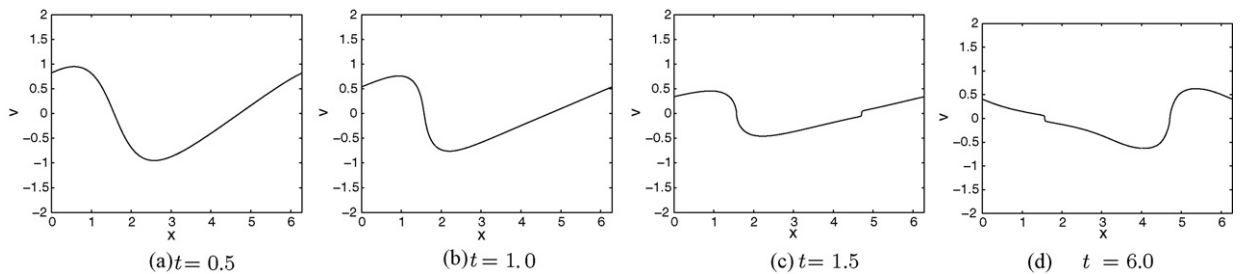


Fig. 6. Evolution of cosine initial data for mCH with $\varepsilon = 0$ and 2π -periodic boundary conditions. Numerical parameters are $N_x = 16,384$ and $dt = 2.5 \times 10^{-4}$.

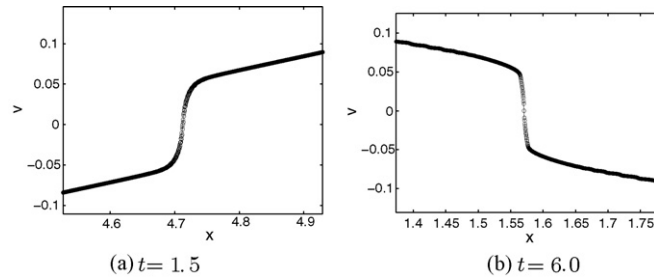


Fig. 7. Magnification of Fig. 6(c) and (d) (mCH with $\varepsilon = 0$, 2π -periodic boundary conditions, $N_x = 16,384$, and $dt = 2.5 \times 10^{-4}$).

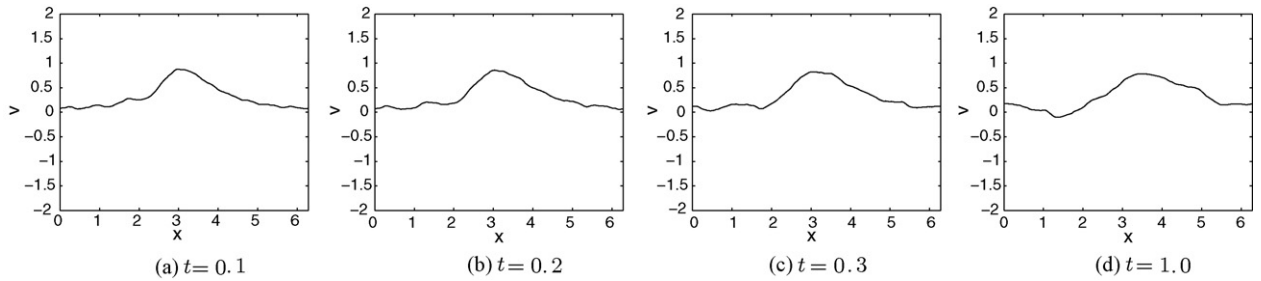


Fig. 8. Evolution of peakon initial data for mCH with $\varepsilon = 10^{-1}$ and 2π -periodic boundary conditions. Numerical parameters are $N_x = 1024$ and $dt = 2.5 \times 10^{-4}$.

into a small kink. This then progresses, at $t = 6.0$, to a different steepened/kink profile which is similar to that at $t = 1.5$ but with reversed symmetry. Please see Appendix A for full details of this evolution. Once again, the magnifications in Fig. 7 show that this is a well-converged solution.

3.4. Numerical simulations: peakon profile

The second set of numerical experiments concern the evolution of a peakon initial profile, (2.1), in the mCH equation which, for the CH equation, has the exact solution (2.2). For this series of trials the discontinuity in the first derivative of the initial data has strong consequences for the numerical simulations. In particular, as the Fourier coefficients of such functions decay quite slowly, one must anticipate that successfully resolving them will require a relatively large number of collocation points. Additionally, as the rate of convergence of spectral methods depends in a fundamental way on the smoothness of the underlying solution, there will not be the exponential rate of convergence observed in Table 2.

The case $\varepsilon = 10^{-1}$ was, quite surprisingly, another very difficult computation. While for time $T = 1.0$, one can realize an error of 0.000572246 with $N_x = 1024$ and $N_t = 4000$, it was impossible to extend this calculation much beyond this time, even with $N_x = 16,384$ points. Fig. 8 displays plots of the peakon solution evolving in mCH with $\varepsilon = 10^{-1}$ for

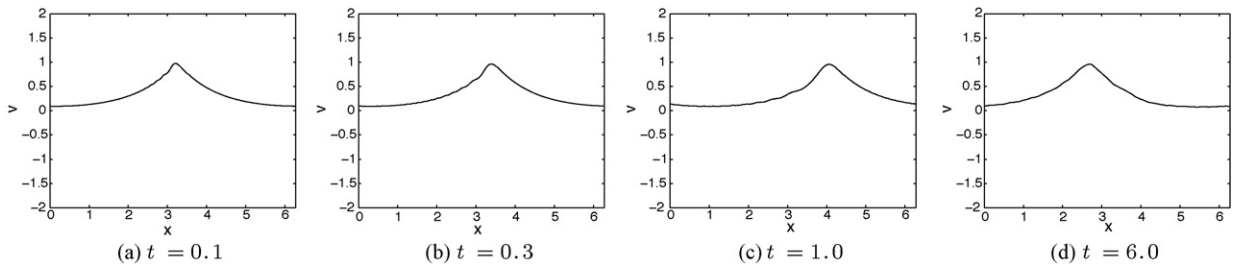


Fig. 9. Evolution of peakon initial data for mCH with $\varepsilon = 10^{-3}$ and 2π -periodic boundary conditions. Numerical parameters are $N_x = 2048$ and $dt = 2.5 \times 10^{-4}$.

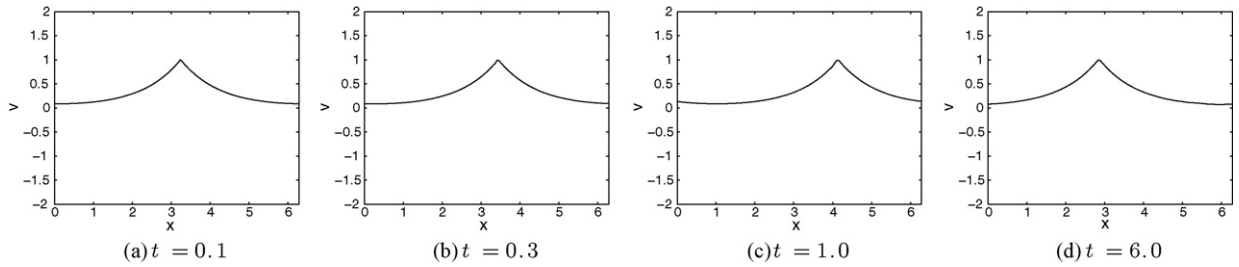


Fig. 10. Evolution of peakon initial data for mCH with $\varepsilon = 10^{-5}$ and 2π -periodic boundary conditions. Numerical parameters are $N_x = 2048$ and $dt = 2.5 \times 10^{-4}$.

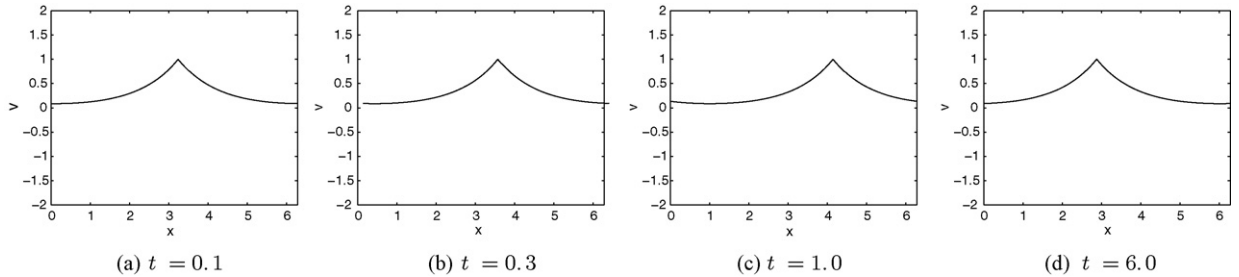


Fig. 11. Evolution of peakon initial data for mCH with $\varepsilon = 0$ and 2π -periodic boundary conditions. Numerical parameters are $N_x = 2048$ and $dt = 2.5 \times 10^{-4}$.

$t = 0.1, 0.2, 0.3,$ and 1.0 ; it is clear from these that the large dispersion quickly destroys any resemblance of the solution to the original peakon.

The case $\varepsilon = 10^{-3}$ was, once again, a challenging computation, however, we were able to extend it all the way to $T = 6.0$ with a reasonable number of discretization points, $N_x = 2048$; with $N_x = 2048$ and $N_t = 24,000$ one can find an error of 0.000257817. Fig. 9 depicts the evolution at the times $t = 0.1, 0.3, 1.0,$ and 6.0 . Here the initial profile appears to “smooth” a little while, in contrast to mCH with $\varepsilon = 10^{-1}$, retaining many of the basic features of the peakon.

Moving to the case $\varepsilon = 10^{-5}$, the results look very similar to the ones outlined above in the case $\varepsilon = 10^{-3}$. Again, solutions could be found all the way to $T = 6.0$ with $N_x = 2048$ collocation points, however, the accuracy was somewhat less refined as $N_x = 2048$ and $N_t = 24,000$ delivered an error of 0.00230018. Fig. 10 shows results of a peakon evolving in mCH with $\varepsilon = 10^{-5}$ at times $t = 0.1, 0.3, 1.0,$ and 6.0 . Here there is no appreciable smoothing of the solution and it appears that the peakon is actually quite close to an exact traveling solution of the mCH equation for this value of the dispersion.

To close we consider the peakon initial condition evolving in the CH equation. Once again, one can follow the solution all the way to $T = 6.0$ with little difficulty though, again, $N_x = 2048$ and $N_t = 24,000$ are required to deliver an error of 0.00278471. Fig. 11 presents results of a peakon evolving in CH at times $t = 0.1, 0.3, 1.0,$ and 6.0 . Here the exact traveling solution appears to be evolving correctly in the CH equation. As a final note, since the peakons are exact traveling solutions of the CH equation for this initial data, the *exact* error can be computed. These errors were comparable to those computed from (3.2) giving us further confidence in both the numerical scheme and our method for verifying it.

4. Conclusions

In this paper we have presented a sophisticated Fourier spectral collocation, Integrating-Factor, fourth order Runge-Kutta method for approximating solutions of the modified Camassa–Holm equation, (1.4). This new algorithm has been tested with two initial profiles (cosine and peakon) with quite different smoothness properties, and four values of the dispersive parameter ε approaching, and including, zero.

To study the limit of mCH to CH as $\varepsilon \rightarrow 0$ we now collect, for both profiles, plots of the solution at a time *well before* the end of our simulations for each of $\varepsilon = 10^{-1}, 10^{-3}, 10^{-5},$ and 0 . These appear in Fig. 12 for the cosine profile, and in Fig. 13 for the peakon profile. From these one can conclude that for this “sufficiently small” time there does appear to

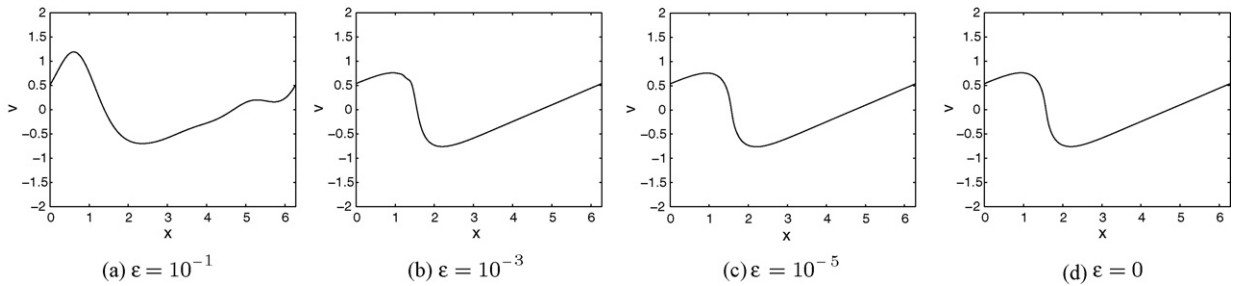


Fig. 12. Evolution of cosine initial data at $t=1.0$ for mCH for varying ϵ and 2π -periodic boundary conditions.

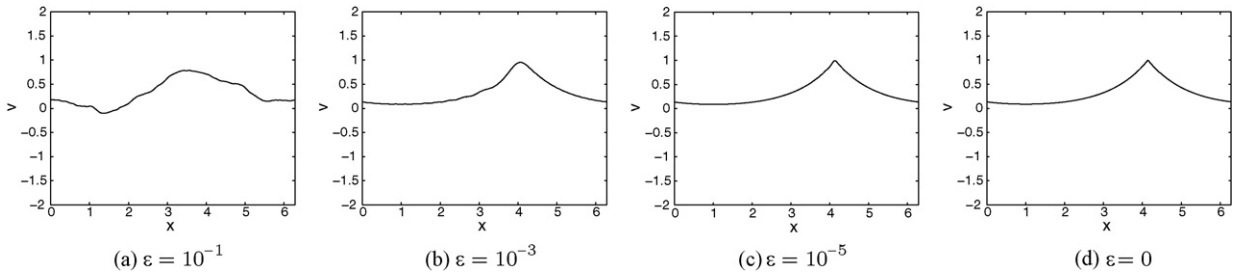


Fig. 13. Evolution of peakon initial data at $t=1.0$ for mCH for varying ϵ and 2π -periodic boundary conditions.

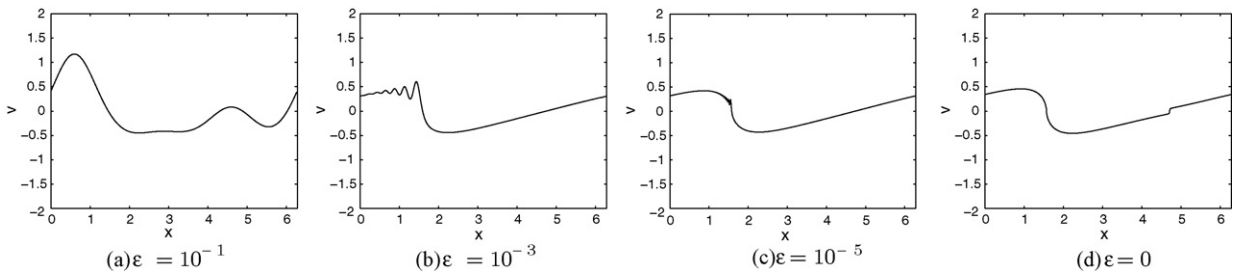


Fig. 14. Evolution of cosine initial data at $t=1.5$ for mCH for varying ϵ and 2π -periodic boundary conditions.

be a limit in L^∞ for all profiles. To decide what the appropriate notion of “smallness” should be for the time variable, Fig. 14 displays plots of the cosine initial data at $t=1.5$ for the four values of ϵ . These are past the “steepening” phase that this solution undergoes for small ϵ . The solutions look quite different and we doubt that a limit exists as $\epsilon \rightarrow 0$ for t beyond steepening. However, the situation is quite different for the peakon initial data which has much weaker smoothness. In Fig. 15 we reproduce the peakon evolution at $t=6.0$ for three values of ϵ (recall that the peakon was not properly resolved in mCH for $\epsilon=10^{-1}$ at $t=6.0$) and notice what appears to be L^∞ convergence as $\epsilon \rightarrow 0$. Here, as there is no steepening, perhaps one does not need to make a smallness assumption on t .

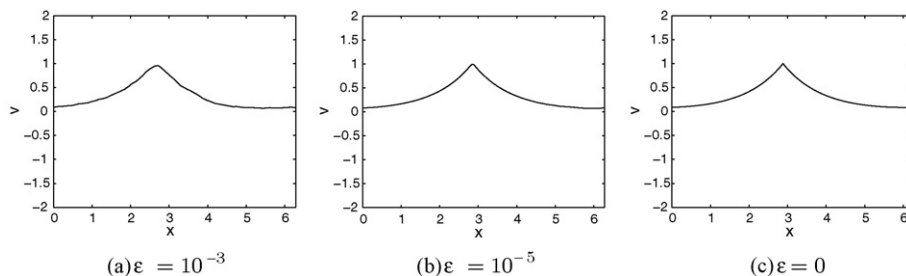


Fig. 15. Evolution of peakon initial data at $t=6.0$ for mCH for varying ϵ and 2π -periodic boundary conditions.

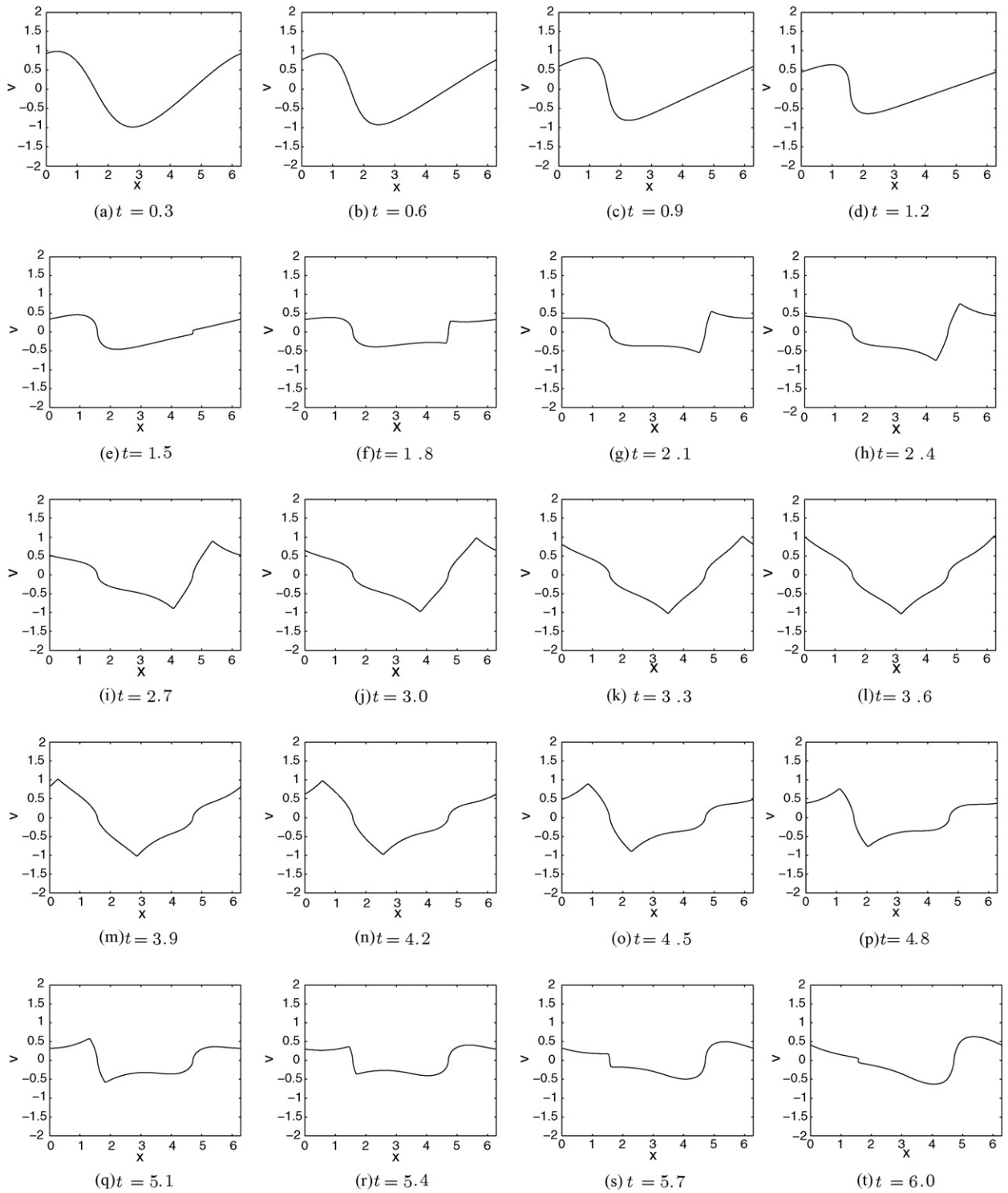


Fig. 16. Evolution of cosine initial data in CH for 2π -periodic boundary conditions ($t=0.3, \dots, 6.0, N_x=16,384, dt=2.5 \times 10^{-4}$).

Thus, in both cases there appears to be an L^∞ limit of our mCH equation to the CH equation as $\varepsilon \rightarrow 0$, provided that t is sufficiently small. For the smooth profile it appears that this t must be chosen *before* the solution approaches steepening. By contrast, beyond this time there appears to be *no* limit as $\varepsilon \rightarrow 0$. However, for the peakon profile this limit does appear to exist in L^∞ for all times considered despite its lack of smoothness.

Appendix A. Evolution of cosine profile in CH equation

In this appendix, we present our full set of numerical results for the case of the cosine profile evolving in the CH equation (see Section 3.3 and Figs. 6 and 7). In contrast to the other solutions presented in this paper, the evolution of v from $t = 1.5$ to $t = 6.0$ in this configuration is by no means clear. In Fig. 16, a “kink” enters the solution, then grows, gradually evolves to a “kinked sawtooth” configuration, and then progresses back to a steepened/kink profile. The interesting feature of these final pictures is that they appear to be mirror images of the solution just before steepening, say at $t = 1.5$. For instance, the placement of the kink and sharp gradient at $t = 6.0$ appear reversed from the solution at $t = 1.5$. As before, the numerical parameters are $N_x = 16,384$ and $dt = 2.5 \times 10^{-4}$ (see Section 3.3).

References

- [1] S. Abenda, T. Grava, C. Klein, On Whitham equations for Camassa–Holm, in: “WASCOM 2005”—13th Conference on Waves and Stability in Continuous Media, pages 1–6, World Sci. Publ., Hackensack, NJ, 2006.
- [2] S. Abenda, T. Grava, Modulation of Camassa–Holm equation and reciprocal transformations, *Ann. Inst. Fourier (Grenoble)* 55 (6) (2005) 1803–1834.
- [3] M.J. Ablowitz, H. Segur, Solitons and the Inverse Scattering Transform, Volume 4 of SIAM Studies in Applied Mathematics, Society for Industrial and Applied Mathematics (SIAM), Philadelphia, PA, 1981.
- [4] J. Bourgain, Fourier transform restriction phenomena for certain lattice subsets and applications to nonlinear evolution equations. I. Schrödinger equations, *Geom. Funct. Anal.* 3 (2) (1993) 107–156.
- [5] J. Bourgain, Fourier transform restriction phenomena for certain lattice subsets and applications to nonlinear evolution equations. II. The KdV-equation, *Geom. Funct. Anal.* 3 (3) (1993) 209–262.
- [6] R. Camassa, D. Holm., An integrable shallow water equation with peaked solitons, *Phys. Rev. Lett.* 71 (1993).
- [7] C. Canuto, M. Yousuff Hussaini, A. Quarteroni, T.A. Zang, Spectral Methods in Fluid Dynamics, Springer-Verlag, New York, 1988.
- [8] A. Constantin, J. Escher, Well-posedness, global existence and blowup phenomena for a periodic quasi-linear hyperbolic equation, *Commun. Pure Appl. Math.* 51 (1998).
- [9] A. Constantin, H. McKean, A shallow water equation on the circle, *Commun. Pure Appl. Math.* 52 (1999).
- [10] S.M. Cox, P.C. Matthews, Exponential time differencing for stiff systems, *J. Comput. Phys.* 176 (2) (2002) 430–455.
- [11] R. Danchin, A few remarks on the Camassa–Holm equation, *Diff. Integr. Eq.* 14 (8) (2001) 953–988.
- [12] B. Fuchssteiner, A. Fokas, Symplectic structures, their Bäcklund transformations and hereditary symmetries, *Physica D* 4 (1981–1982) 47–66.
- [13] J. Gorsky, On the Cauchy problem for a KdV-type equation on the circle. PhD thesis, University of Notre Dame, 2004.
- [14] J. Gorsky, A. Alexandrou Himonas, Well-posedness for a class of nonlinear dispersive equations, *Dyn. Contin. Discrete Impuls. Syst. Ser. A Math. Anal.* 14 (Advances in Dynamical Systems suppl. S2) (2007) 85–90.
- [15] D. Gottlieb, S.A. Orszag. Numerical analysis of spectral methods: theory and applications. Society for Industrial and Applied Mathematics, Philadelphia, PA, 1977. CBMS-NSF Regional Conference Series in Applied Mathematics, No. 26.
- [16] A.A. Himonas, G. Misiołek, Well-posedness of the Cauchy problem for a shallow water equation on the circle, *Journal of Differential Equations* 161 (2000).
- [17] A.A. Himonas, G. Misiołek, The Cauchy problem for an integrable shallow-water equation, *Diff. Integr. Eq.* 14 (7) (2001) 821–831.
- [18] A.A. Himonas, G. Misiołek, High-frequency smooth solutions and well-posedness of the Camassa–Holm equation, *Int. Math. Res. Not.* 51 (2005) 3135–3151.
- [19] R.S. Johnson, Camassa–Holm, Korteweg–de Vries and related models for water waves, *J. Fluid Mech.* 455 (2002) 63–82.
- [20] C.E. Kenig, G. Ponce, L. Vega, A bilinear estimate with applications to the KdV equation, *J. Am. Math. Soc.* 9 (2) (1996) 573–603.
- [21] P. Lax, D. Levermore, The zero dispersion limit for the Korteweg–de Vries (KdV) equation, *Proc. Natl. Acad. Sci. U.S.A.* 76 (1979).
- [22] P.D. Lax, C.D. Levermore, The small dispersion limit of the Korteweg–de Vries equation. I, *Commun. Pure Appl. Math.* 36 (3) (1983) 253–290.
- [23] P.D. Lax, C.D. Levermore, The small dispersion limit of the Korteweg–de Vries equation. II, *Commun. Pure Appl. Math.* 36 (5) (1983) 571–593.
- [24] P.D. Lax, C.D. Levermore, The small dispersion limit of the Korteweg–de Vries equation. III, *Commun. Pure Appl. Math.* 36 (6) (1983) 809–829.
- [25] G. Misiołek., Classical solutions of the periodic Camassa–Holm equation, *Geom. Funct. Anal.* 12 (5) (2002) 1080–1104.
- [26] L. Molinet, On well-posedness results for Camassa–Holm equation on the line: a survey, *J. Nonlinear Math. Phys.* 11 (4) (2004) 521–533.
- [27] D. Sattinger, R. Beals, J. Szmigielski, Multi-peakons and a theorem of Stieltjes, *Inverse Problems* 15 (1999).